Analysis of the hydraulic fracturing behaviour in the Bowen Basin (Australia)

by

H. Morales[1] and S. Davidson[2]

[1]Dowell Schlumberger, [2]Jadmist Pty Limited

ABSTRACT

This paper presents an analysis of the hydraulic fracturing stimulations of the coalbed formations of the Bowen Basin of eastern Australia. In particular, two fracturing tests conducted in coal seam No. 4 (Well 3) are analyzed.

The analysis indicates that multiple fractures with horizontal and vertical components are created. A pressure-dependent fluid-loss formulation for naturally fractured reservoirs and a large apparent fracture toughness are necessary to match the observed pressures.

A calibration treatment to determine the fracturing regimes, pressure-dependent permeability, and apparent fracture toughness is proposed for the design and analysis of forthcoming fracturing stimulations. The formulations for these mechanisms are described.

INTRODUCTION

Several wells have been hydraulically fractured during the last five years in the Moranbah and Baralaba coal measures of the eastern Bowen Basin of Australia[1-4] (shown on the map of Figure 1). The depths of the coalbed formations are relatively shallow (1,290 ft to 1,650 ft) and the coal formation heights are small (5 ft to 16 ft)[2-4].

With a few exceptions, the fracture-pressure gradients (1.5 to 2.15 psi/ft) are greater than the overburden gradient. Typically, the fluid pressure increases during the early stages (one to two minutes) of pumping and decreases thereafter. Closure-pressure gradients of 0.77 psi/ft to 1.16 psi/ft have been inferred from the postfracture pressure decline analysis[1-4].

The presence of multiple fractures is expected in the stimulation of coal seams at high pressures. For example, two vertical fractures (orthogonal to each other) within the coal seam were observed in the mineback test of the German Creek mine[11]. The German Creek mine is located in the southeast section of the Bowen Basin. Further, traces of vertical fractures were found in the caprock. The coal fractures and the caprock fractures were not clearly connected. Additionally, fluid traces were found in an existing horizontal shear fault near the coal/caprock interface.

WELL 3 HYDRAULIC FRACTURING EXPERIMENTS

Minifrac and main fracturing tests were conducted in December 1990 in coal seam No. 4 (Well 3) of the Baralaba coal measures. The mechanical properties and other formation parameters are listed in Table 1.

A 32-lb borate crosslinked pumping fluid was used for all tests. The fluid and proppant volumes for the main fracturing treatment are listed in Table 2.

The description, data collection, and pressure analysis for these tests are outlined in References 3 and 4. However, the analysis performed in these reports is based on established principles for sandstone formations and cannot be used to explain the pressure response observed during pumping. As shown in this paper, the use of multiple fracturing mechanisms, pressure-dependent fluid loss, and apparent fracture toughness is necessary to explain and reproduce the field-recorded pressures.

MINIFRAC TEST ANALYSIS

A minifrac test was conducted with the purpose of measuring the fluid-loss coefficient and closure pressures. 26,400-gal of borate-crosslinked fluid was pumped at 25 bpm through the annulus. The pressures were monitored in the annulus (dead string). The

plot of the surface pressure vs. pumping (and shut-in) time depicted in Figure 2 shows a pressure increase to 1,850 psi during the first two minutes of pumping. Thereafter, the pressure decreases continuously to 1,650 psi at shut-in.

MINIFRAC - MODELING

Figure 2 also compares the pressures obtained using a multiple fracture simulator with the field-recorded pressures. The dotted line is the pressure obtained from the model. A finite element analysis indicated that equivalent Young's modulus greater than the coal modulus was necessary to consider the influence of the barrier stiffness. Accordingly, Young's moduli of 550,000 psi and 2,300,000 psi, were used for the vertical and horizontal fractures, respectively.

Further, an apparent fracture toughness which is approximately two orders of magnitude larger than the laboratory-measured fracture toughness for coal specimens[12] (100 to 500 psi $in.^{1/2}$) was used to match the field pressures. The apparent fracture toughness is intended to represent the effects of a lag region that is not significantly penetrated by the fluid and/or a process zone that is generated around the crack tip[5-7].

Figure 3a compares the pressures estimated by using a fracture toughness of 500 psiin. with the pressures obtained by using the larger apparent fracture toughness. The former case underestimates the field pressures by 63%, while the fracture length is overestimated by 12%.

MINIFRAC - FRACTURING REGIMES

As shown in Figure 2, two distinct fracturing regimes can be interpreted from the observed and modeled pressures. The first one is the steep pressure increase which occurs during the first two minutes of pumping and corresponds to the lateral extension of a vertical fracture contained in the coal seam No. 4. The second is a decreasing pressure trend which corresponds to the radial extension of a horizontal fracture (at the upper or lower coal-barrier interface). Because of the smaller pressures required to propagate a radial fracture (compared to the pressures required to propagate the contained vertical fracture), the radial extension of the horizontal fracture occurs at the expense of small or no propagation of the vertical fracture.

MINIFRAC - PRESSURE-DEPENDENT FLUID-LOSS

The pressure plots in Figures 2 and 3b show a decrease in the slope at the breakover point between geometries (i.e., segment A-B in Figure 2). Further, the postshut-in falloff data contained in Figure 4a shows a nonlinear response after shut-in immediately followed by a linear response. The decrease in pressure slope during pumping and the nonlinear/linear response after shut-in are pressure-dependent fluid loss trends.

The decrease in slope (A-B) is modeled as an increase in fluid loss (caused by an increase in cleat aperture) with increase in fluid pressure. The nonlinear response is modeled as leakoff from the closing fissures and the linear response as leakoff from the matrix.

Figure 3b, which shows a comparison between conventional (broken line) and pressure-dependent (solid line), fluid-loss formulations, indicates that the conventional fluid-loss modeling overestimates the pressures at critical intervals. A fluid-loss coefficient of 0.0049 ft/min (Jeffrey[3]) is used for the constant fluid-loss modeling, while the Walsh criterion (given by Equation 2) is used to relate the permeability to the fluid treating pressure. The evaluation of the Walsh equation and the pressure-dependent modeling are described later in this paper.

Based on the analysis described above, a 290-ft fracture half-length and an 82-ft radial extension are estimated for the vertical and horizontal fractures, respectively. The estimated wellbore openings in the vertical and horizontal fractures are 0.30 in. and 0.84 in., respectively.

The postshut-in pressure decline (Figures 4a and 4b) shows an inflection point at 1,730-psi bottomhole pressure which can be interpreted as the closure of the horizontal fracture, and a second inflection point at 1,340

psi which can be interpreted as the closure of a vertical fracture.

MAIN FRACTURING TEST

The main fracturing test consisted of pumping 111,000 gal of 32-lb crosslinked borate and 123,100 lb of proppant. Because of equipment problems, only a fraction of the scheduled volume (75,000 gal of fluid and 63,500 lb of proppant) was pumped the first day (Feb. 17, 1990), in three pumping phases. The remaining volume was pumped the following day. Table 2 lists the rates and slurry volumes used in the four phases. The main events are outlined below but Reference 3 describes the fracturing procedures in detail.

The first pumping phase terminated after 48 min because of anomalies in the densitometer gauge. The second phase consisted of 6-1/2 min of fluid injection to clean and circulate the slurry from the blender and tubulars. In the third phase, proppant was ramped from 0.47 to 3.75 ppg within a 28-min interval. At this time, a steep increase in pressure (interpreted as a near wellbore screenout) occurred. Reference 3 indicates that a failure in the cross-linked activator likely caused the wellbore screenout. The next day pumping was resumed by ramping the proppant from 0 to 4.58 ppg within a 35-min time interval. Pumping was terminated after a tip screenout occurred.

OBSERVED PRESSURES

Similar pressure trends to the ones observed in the minifrac test are seen in the main fracturing test. For example, Figure 5a shows that the surface pressure increases to 1,800 psi during the earlier stages (0 to 2 min) of pumping. Thereafter, the pressure decreases to approximately 1,500 psi (end of first pumping phase). After shut-in, the pressure decreases to 1,100 psi. A pressure increase to 1,450 psi is observed during the 6.5 min of injection in the second phase. Except for the intervals of pressure rise observed at the end of Phases 3 and 4 (caused by wellbore bridging and tip screenout, respectively), the same sequences of events, already for the minifrac are observed in these pumping phases.

MAIN FRACTURING TREATMENT MODELING - PHASES 1 TO 3

The multiple fracture, apparent fracture toughness, and pressure dependent fluid loss schemes described later in this paper are used to model the four phases of the main fracturing test.

The observed and modeled pressures (Figure 5a) indicate that the vertical and horizontal fractures created in the minifrac test were reopened and propagated in Phases 1 and 3. Phase 2 (which was used to circulate fluid) did not affect the pressure response nor the fracture propagation.

The pressure behavior predicted by the model (dotted line) follows closely the field-recorded pressures (solid line) and has similar characteristics to the minifrac test. However, as described in the following section, the propagation of a new horizontal fracture is likely to have occurred in Phase 4.

A 290-ft one-wing vertical fracture and a 100-ft radius horizontal fracture are estimated for the first pumping phase. No significant fracture advancement occurred in the second phase. However, the radial extension was increased to 130 ft during the third phase, while the vertical fracture remained unchanged. Hydraulic wellbore openings of 0.32 in. (for the vertical fracture) and 0.98 in. (for the horizontal fracture) are estimated. Only the horizontal fracture was propped. Propped radii of 30 ft and 80 ft are estimated for Phases 1 and 3, respectively. A propped width of 0.297 in. (3.15 psf) is estimated at the end of Phase 3.

MAIN FRACTURING TREATMENT MODELING - PHASE 4

A finite-element analysis indicates that the formation displacement imposed by the propped width in coal seam No. 4 increases the localized in-situ stresses by approximately 100 psi for each 0.1 in. Therefore, the fracture reopening pressure (of a propped fracture) is expected to be greater than the reopening pressure of a nonpropped fracture. Further, if fracture reopening occurs, the residing proppant will be carried by the pad causing premature fracture screenout.

The pressure behavior observed in Phase 4 (Figure 5b) is consistent with the reopening and propagation of the existent vertical fracture and the development of a new horizontal fracture, i.e., the opening pressure for the horizontal fracture is approximately equal to that observed in Phases 1 and 3 and the screenout time is consistent with that of a newly propagated fracture (no contribution of residing proppant).

The screenout condition, depicted by the pressure rise at the end of Phase 4, is characterized by a steep slope (4:1 in Figure 7b) caused by fluid storage (in a stationary fracture) and frictional resistance (in a rapidly dehydrating fracture). The fluid dehydration is caused by the increase in fluid loss with the increase in pressure.

As explained in later, the log-log plots of net pressure vs. pumping time for each geometry (Figures 6a and 6b respectively), follow the expected trends for PKN and radial fractures. Based on the modeling results the vertical fracture was propagated to approximately a 300-ft one-wing length (0.33 in. wellbore opening), while a 100-ft fracture radius is estimated for the new horizontal fracture (0.94 in. wellbore opening). At the end of pumping, the estimated propped radius is approximately equal to the fracture radius (100 ft). A propped width of 0.179 in. (1.89 psf) is estimated for the horizontal fracture. It is likely that the vertical fracture was propped in the vicinity of the wellbore during the high-pressure interval.

CALIBRATION TREATMENT

To design and analyse forthcomimg fracturing stimulations, it is proposed to use a fracturing calibration treatment with the same fluid and the same injection rates as those selected to carry the proppant to determine" (1) the signatures depicting the fracturing regimes, (2) the apparent fracture toughness that matches the field pressures, and (3) the relation between pressure and permeability (to model the fluid loss through the natural fissures).

The following sections describe the behavior of the fracturing regime signatures, pressure dependent permeability, apparent fracture toughness, and multiple fractures.

FRACTURING REGIME SIGNATURES

The pressure trends observed from a log-log plot of pressure vs. pumping time are indicative of the fracturing regimes occurring during the pumping process. For example, the relation of wellbore pressure to the pumping time (derived from the equations for fluid flow, solid deformation, and material balance) for the three basic fracturing models (PKN, KGD, and radial) can be expressed by the proportionality[13]

$$\log p_{net} \propto b \log t \,, \qquad (1)$$

where t is the fracture propagation time (for each fracture component) and b is the slope of a log p_{net} vs. log t plot. The value of b depends on the fracture geometry, fluid rheology, and efficiency.

For a PKN fracture,

b = 1/[4(n'+ 1)] (low efficiency),

b = 1/(2n'+ 3) (high efficiency).

For a radial model,

b = -3n'/[8(n'+ 1)] (low efficiency),

b = -n'/(n'+ 2) (high efficiency).

For a KGD model,

b = -n'/[2(n'+ 1)] (low efficiency),

b = -n'/(n'+ 2) (high efficiency).

In general the slope b of a log-log pressure vs. time plot is related to the fracture behavior as follows ---

- a positive b (less than one) indicates lateral extension in a contained or partially contained fracture.
- due to increase in fissure aperture, b can decrease from a positive value (i.e., 1/4 to 1/8) to a smaller value (i.e., zero);
- a negative b indicates uncontained fracture extension (i.e., penny-shaped or KGD fracture growth);
- b approaches a value of one in a fracture in which fluid storage occurs (i.e., growth restriction due to screenout); and

- after screenout, b can further increase to values greater than one with fluid dehydration.

The above pressure trends are illustrated in Figures 6a and 6b. The initial pressure interval of Figure 6a follows a slope of 1:4.4. This slope is consistent with a PKN fracture, and corresponds to the propagation of a contained vertical fracture. With pumping time the slope decreases to approximately zero. The decrease in slope can be attributed to the enhanced fluid loss caused by the fissure aperture increase. At approximately 2.3 min of pumping, the slope changes from positive to negative. This time is considered the initiation time for the horizontal fracture, i.e., the bottomhole pressure gradient of 1.3 psi/ft (2,570 psi bottomhole pressure) is greater than the overburden pressure gradient of 1.05 psi/ft. Figure 6b contains the bottomhole pressure vs. time for the horizontal fracture. The initial pressure interval of Figure 6b shows a negative slope of 1:4.56. This slope is consistent with a radial model, and corresponds to the propagation of a horizontal fracture. After screenout the pressure slope increases to 4:1. The increase in slope indicates a high frictional pressure resistance, within the fracture, caused by proppant dehydration.

PRESSURE-DEPENDENT PERMEABILITY FOR NATURALLY FRACTURED RESERVOIRS

Figure 7 illustrates the fluid-loss behavior of a hydraulic fracture propagating within a naturally fractured reservoir. For this fracture, the most significant fluid loss occurs through the fissures normal to the fracture at fluid pressures approaching the fissure's closing pressures (σ_{hmax}).

The Walsh criterion[14] provides an excellent representation of the permeability vs. pressure response for a fracture intercepting natural fissures. The Walsh equation is given by[15]

$$k = k_o[D \ln\frac{\sigma^*}{\sigma - p}]^3 , \quad (2)$$

where k is the permeability at a reservoir pressure p, k_o is a reference permeability, D is a constant, σ^* is a reference state of stress, and σ is the stress normal to the fissures. Equation 2 indicate that for fluid pressures approaching the fissure closure stresses (σ-p= 0), the permeabilities are several orders of magnitude larger than the permeabilities at small or no fluid pressures (σ-p= σ_{hmax}). Two points (k_i,p_i) are necessary to evaluate the parameters D and σ^* As explained below, the Walsh equation or similar function is required for the fluid-loss evaluation of naturally fractured reservoirs.

PRESSURE-DEPENDENT PERMEABILITY IN FLUID-LOSS MODELING

A formulation to measure fluid loss in naturally fractured reservoirs based on the Walsh criterion and Darcy's law is outlined in Reference 15. The analysis assumes that the fissures have a constant area in a gas reservoir, and the influence of back stresses caused by the pore-pressure increase is ignored. The basic equations are summarized below.

The fluid-loss velocity which constitutes the principal equation to estimate the fluid-loss volume is given by

$$v = \frac{C(p)}{\sqrt{t}} , \quad (3)$$

where

$$C(p) = \alpha\,[F(p_r) - F(p_f)]^{1/2} , \quad (4)$$

$$\alpha = \sqrt{\frac{k_o \phi D^3}{\mu g}} , \quad (5)$$

and

$$F(p) = (\sigma - p)\,[(\ln\frac{\sigma^*}{\sigma - p})^3 + 3(\ln\frac{\sigma^*}{\sigma - p})^2 + 6(\ln\frac{\sigma^*}{\sigma - p}) + 6] \quad (6)$$

where μ is the viscosity for the fracturing fluid, ϕ is the formation porosity, p_r is the reservoir pressure, p_f is the fluid pressure and g is a factor to account for non-constant leakoff velocity along the fissure (g is close to unity for most cases). Equations 3 through 6 are sufficient to estimate the fluid-loss volume by integrating the fluid velocity over the fracture area.

PRESSURE DECLINE ANALYSIS

Based on the analysis outlined above, an inverse scheme can be used to back calculate the permeability from a calibration treatment by evaluating the parameters D and σ^* from the pressure decline after shut-in.

From material balance after shut-in, the fluid-loss rate q_{lt} can be defined in terms of the G function as follows (7)

$$q_{lt} = \frac{2C(p)A_p}{\sqrt{t_p}} G(\Delta t_D) ,$$

where A_p is the area obtained at the end of pumping (assumed to be constant during fracture closure), and t_p is the pumping time. Further, the average fracture opening can be defined in terms of the fracture compliance, c_f.

(8)

$$w = c_f (p_f - p_c) ,$$

where (9)

$$c_f = \frac{\pi\beta}{2E'} M .$$

In Equations 8 and 9, p_f is the fluid pressure, p_c is the closure pressure, β is the ratio of the average fracture pressure to the wellbore pressure, and E' is the plane strain Young's modulus. M is a model-dependent factor equal to ----

- h_f for a PKN model,
- $2x_f$ for a KGD model, and
- $32R/(3\pi^2)$ for a radial model.

By combining Equations 7 through 9 and integrating the resulting expression over two shut-in times, i.e., Δt_1 and Δt, an expression relating the pressure-dependent function F(p) to the G function is obtained (10)

$$-\int_{p_f(\Delta t_1)}^{p_f(\Delta t)} \frac{dp_f}{[F(p_c)-F(p_f)]^{1/2}} = \frac{r_p\sqrt{t_p}\pi\alpha}{2c_f} G(\Delta t_1,\Delta t) ,$$

where r_p is the ratio of the fluid-loss area to the fracture area. The G function has been defined[13] for two limiting conditions, i.e., for a high-efficiency fracture, (11)

$$G(\Delta t_D) = \frac{16}{3\pi}[(1+\Delta t_D)^{3/2}-\Delta t_D^{3/2}-1] ,$$

and for a low-efficiency fracture, (12)

$$G(\Delta t_D) = \frac{4}{\pi}[(1+\Delta t_D)\sin^{-1}(1+\Delta t_D)^{-1/2}+\Delta t_D^{1/2}-\frac{\pi}{2}] .$$

From Equation 10, α can be written as follows, (13)

$$\alpha = -\frac{2(LHS)c_f}{\pi r_p\sqrt{t_p}G(\Delta t_1,\Delta t)} .$$

Equations 4, 10, and 13 are used to evaluate the parameters D and σ^*, from the early falloff data, by using the following iterative procedure ----

1) assume values for σ^* and C;

2) use Equation 10 and Equation 13 to evaluate α at two points of the pressure-decline plot;

3) calculate a new value for D from Equation 4;

4) use D to obtain a new value for σ^* by satisfying Equation 10;

5) check if Equation 10 is satisfied (within a convergence criteria) at a neighboring point of the pressure-decline plot;

6)correct σ^*; and

7)repeat Steps 2 through 6 until convergence is achieved.

Alternatively, measurements for permeability and pressure from drawdown tests or laboratory measurements can be used to evaluate the parameters D and σ^*.

Signatures indicating pressure-dependent permeability in the pressure vs. time plot of a fracturing treatment include ----

- a critically enhanced fluid loss at fluid pressures close to (or greater than) the fissure closure pressures - this condition is depicted by a decrease in the slope of a pressure vs. time plot of a contained fracture (i.e., segment A-B of Figure 2);
- a nonlinear response followed by a linear response in the plot relating the pressure decline after shut-in to the closure time (Figure 4a); and
- relatively long closure times, providing a false indication of a higher efficiency.

APPARENT FRACTURE TOUGHNESS

Experimental data indicate that fracture toughness values for coal can vary between[12] 90 psi $in.^{1/2}$ and 500 psi $in.^{1/2}$ The representative value of 100 psi $in.^{1/2}$ for friable coals is about one order of magnitude smaller than the fracture toughness values for most sandstones.

The effect of using laboratory-measured fracture toughness values in modeling applications is minor compared to the case which ignores fracture toughness. For instance, calculations for contained fractures using fracture toughness values of 1,000 psi $in.^{1/2}$ show a 0.1% increase in net pressure compared to the case which ignores the rock toughness effect.

To bring the net pressure to values comparable with the field-recorded pressures, apparent fracture toughness values greater than one order of magnitude larger than the laboratory-measured values have been suggested[5,6]. The fracturing behavior obtained with a large apparent fracture toughness value is expected to equivalently reproduce the behavior resulting from tip fracturing mechanisms (such as a lag zone and/or a process zone[5-7]).

A tip-pressure boundary condition can be used to estimate the apparent fracture toughness by noting that a large fracture toughness, process zone, and/or a lag zone result in an increased tip pressure[7]. In a small fracturing treatment (calibration treatment) the wellbore pressure is approximately equal to the tip pressure. Thus the pressure obtained immediately after shut-in provides a close estimate of the tip pressure, p_o, because the frictional effects in the tubing and perforations are already dissipated, i.e.,

$$p_o = ISIP - p_c \,, \tag{14}$$

where ISIP is the instantaneous shut-in pressure, and p_c is the closure pressure. Further the tip pressure is related to the apparent fracture toughness, K_{ap}, by the following expression

$$K_{ap} = \frac{2}{\pi} p_o \sqrt{R} \,, \tag{15}$$

where R is the radius of a penny-shaped fracture. The evaluation of K_{ap} requires the knowledge of p_o (from a calibration treatment) and of the fracture radius, R. A value of R equal to one-half of the height of a contained fracture will provide a conservative estimate. Alternatively, R can be estimated from a hydraulic fracturing model. A tip pressure evaluated from a calibration treatment can be used as a boundary condition to represent an equivalent fracture toughness.

The above analysis, which is based on a radial fracture model, has been expanded by Nolte[17] to a contained or partially contained fracture (i.e., P3D model) by noticing that the tip region can be considered a semicircular cap in which a steady-state pressure boundary condition p_o can be imposed. The circular cap is expected to achieve a steady-state condition because the elastic coupling is limited to a distance of the order of the height.

Because the viscous frictional effects are greater in contained fractures than radial fractures, fracture toughness effects are significant for cases in which the viscous net pressure (for a case without toughness) is less than about one-half p_o17

MODELING OF A SYSTEM OF MULTIPLE FRACTURES

To simulate the simultaneous propagation of multiple fractures, it is necessary to integrate the single fracture model with a series of constraints which couple the behavior of individual fractures[18]. In Reference 18, an appropriate set of constraints for PKN fractures was derived by drawing an analogy with an electrical circuit network. This paper expands that scheme to a combination of vertical and horizontal fractures[16].

Figure 8 illustrates an idealized multilayer fracture treatment and the electric circuit analogy to the treatment. Fractures are generated in each of the n layers located at depths z_1 through z_n. The total pumping rate, Q_t, is partitioned into layer pumping rates, Q_1 through Q_n. The conservation of volume implies that

$$Q_t = \sum_{i=1}^{n} Q_i \quad (16)$$

Further, a reference pressure, p_o, is assumed to be recorded at a depth, z_o.

The drop in pressure from z_o to the top of the i_{th} fracture is caused by the casing and/or tubing friction $\Delta p_{pf,i}$; the perforation friction $\Delta p_{fc,i}$; the hydrostatic pressure $\Delta p_{h,i}$; and the net pressure $\Delta p_{w,i}$.

For each fracture the sum of all pressure effects including the closure pressure, p_c, must be equal to

$$p_o = p_{c,i} + \Delta p_{w,i} + \Delta p_{pf,i} - \Delta p_{h,i} + \Delta p_{fc,i} \quad (17)$$

Equations 16 and 17 lead to a system of n+ 1 equations with n+ 1 unknowns (Q_1 through Q_n and p_o).

An initiation criterion must be satisfied before the fracture begins to propagate.

- The initiation criterion for a vertical fracture in the minimum in-situ stress plane is BHP $\geq \sigma_{hmin}$.
- The initiation criterion for a vertical fracture in the maximum in-situ stress plane is BHP $\geq \sigma_{hmax}$.
- The criterion to propagate an already existing horizontal fracture of radius R is BHP $\geq \sigma_v + p_o$.

where σ_v is the overburden stress, and p_o is the tip pressure for a penny-shaped fracture (given by Equation 15) at a given apparent fracture toughness.

CONCLUSIONS

Based on the minifrac and main fracturing tests conducted in coal seam No. 4 (Well 3), the following conclusions can be drawn.

1) The pressure behavior observed during pumping is consistent with a fracturing system composed of vertical and horizontal fractures.

2) Vertical fracture propagation occurred during the early stages of pumping (0 to 2 min). The fracture is likely to be contained within the coal seam as depicted by the positive slope in pressure vs. pumping time plot.

3) It is possible that more than one vertical fracture was propagated during the early stages of pumping (this assumption has been substantiated by mineback observations[11]). However, because of the minor differences between the pressure signatures for one vertical fracture and those for two orthogonal vertical fractures, it is difficult to clearly determine the development of multiple fracture systems.

4) The horizontal fractures are likely to propagate in weak planes (or faults) and are depicted by the negative slope in the pressure vs. pumping time plot. This regime follows the early pressure rise. The horizontal fractures propagate at the expense of the vertical fractures. Only the horizontal fractures are propped during normal pumping conditions. Both the vertical and horizontal fractures are propped during intervals of high-pressure rise (i.e., tip screenouts). However, the propped vertical area is expected to be localized to the vicinity of the wellbore.

5) A large apparent fracture toughness is necessary to match the high pressures resulting from a lag and/or process zone near the crack tip region. In addition an appropriate pressure-dependent permeability relation is necessary to model the enhanced fluid loss caused by the increase in cleat aperture.

6) Signatures exist for pressure behavior after screenout. For example, in the absence of frictional effects, the change to the 1:1 slope is gradual for a contained or partially contained fracture. However, a radial fracture will immediately approach the 1:1 slope. Further slurry dehydration can significantly increase the pressure slope, e.g., a 4:1 slope is observed in the screenout stage of Phase 4 (Figure 6b).

ACKNOWLEDGMENTS

The authors gratefully acknowledge the permission of MIM Holdings Limited and Dowell Schlumberger to publish this paper.

REFERENCES

1) Reeves, S.R.: "Evaluation of Hydraulic Fracturing at the Broadmeadow Field," 1990 Classified NQE Report, July.

2) Reeves, S.R. and O'Neill, P.J.:"Preliminary Results from the Broadmeadow Pilot Project, Bowen Basin, Australia," 1989 Coalbed Methane Symposium, University of Alabama (Tuscaloosa), April 17-20.

3) Jeffrey, R.G.: "An Analysis of the Hydraulic Fracture Stimulation of the coal seam No. 4 in Well 3," 1991 CSIRO Internal Report - New Series No. 44, April.

4) Badri, M.:" Preliminary Frac-Evaluation, Well 3, coal seam No. 4," 1991 NQE Internal Report, v 1, May.

5) Jeffrey, R.G.: "The Combined Effect of Fluid Lag and Fracture Toughness on Hydraulic Fracture Propagation," Paper SPE 18957, 1989 SPE Rocky Mountain Regional Meeting/Low-Permeability Reservoirs Symposium, Denver, CO.

6) Shlyapobersky, J., Wong, G.K., and Walhaug, W.W.: "Overpressure Calibrated Design of Hydraulic Fracture Simulations," Paper SPE 18194, 1988 SPE Annual Technical Conference and Exhibition, Houston, TX.

7) Jones, A.H., Bell, G.H., and Morales, R.H.: "Examination of Potential Mechanisms Responsible for the High Treatment Pressures Observed During Stimulation of Coalbed Reservoirs," Paper SPE 16421, 1987 SPE/DOE Low-Permeability Reservoir Symposium, Denver, CO.

8) Davidson, S.:"Field Report and Preliminary Interpretation for Post-Casing, Pre-Frac Extended Test, Well 3, Coal Seam No. 4," 1991 NQE Report, Jan.

9) Jones, A.H., Bell, G.H., and Morales, R.H.: "Coalbed Hydraulic Fracture Treatment Empirical Relationships and Computer Simulation," Paper SPE 15242, 1986 SPE Unconventional Gas Technology Symposium, Louisville, KY.

10) Morales, R.H.: "Coal Seam No. 4, Well 3 Hydraulic Fracture Design Report," Internal Report prepared for NQE, Nov. 28, 1990.

11) Jeffrey, R.G.: "Hydraulic Fracturing Experiment in Well ECC87 at German Creek Mine Central Collery," CSIRO Division of Geomechanics Preliminary Report 1 (Jan. 1991).

12) Kirby G.C. and Mazur C.J.: "Fracture Toughness Testing of Coal," Proc. 26th Symposium on Rock Mech., Rapid City, SD (1985), 487-504.

13) Nolte, K.G.: "A General Analysis of Fracturing Pressure Decline With Application to Three Models," SPEPE (Dec. 1986) 571-583.

14) Walsh, J.B.: "Effect of Pore Pressure and Confining Pressure on Fracture Permeability," Int. J. Rock Mech. and Min. Sci. Geomech. Abstr. (1981) 18, 429-435.

15) Warpinski, N.R.: "Hydraulic Fracturing in Tight, Fissured Media," JPT (Feb. 1991), 146-152, 208-209.

16) Morales, R.H.: " Coalbed Fracturing Guidelines - Interim Report," DL Report No. 10640, Oct. 21, 1991.

17) Nolte, K.G.: "Fracturing-Pressure Analysis for Nonideal Behavior," JPT (Feb. 1991) 210-218.

18) Elbel, J.L., Piggott, A.R., and Mack, M.G.:"Numerical Modeling of Multilayer Fracture Treatments," Paper SPE 23982, 1992 SPE Permian Basin Oil and Gas Recovery Conference, Midland, TX.

19) Palmer,I.D.: "Review of Coalbed Methane Well Stimulation," Paper SPE 22395, 1992 International Meeting on Petroleum Engineering, Beijing, China.

Formation Properties	Parameter
Coal	
Depth (ft)	1,651.5
Formation Height (ft)	10
Young's Modulus (psi)	300,000
Poisson's Ratio	0.39
Permeability (md)	2.7 to 3.6
Porosity	0.04
Temperature (°F)	100
σ_{hmin} (psi)	1,320
σ_{hmax} (psi)	1,730
Bounding Rocks	
Young's Modulus (psi)	2,320,000
Poisson's Ratio	0.23

Table 1. Formation properties

Test	Stage	Volume (U.S.gal)	Sand (ppg)	Mesh
Main (Phases 1-3)	1	41,454	0	
	2	3,192	0.96	40/70
	3	2,415	0.96	12/20
	4	shut-in		
	5	2,709	0	
	6	shut-in		
	7	5,367	0.47	12/20
	8	4,888	1.59	12/20
	9	4,439	2.68	12/20
	10	8,266	3.29	12/20
	11	2,331	3.75	12/20
Main (Phase 4)	1	12,705	0	
	2	6,237	0.54	12/20
	3	4,267	1.48	12/20
	4	6,468	3.22	12/20
	5	6,346	4.58	12/20

Notes:
1) Main (Phases 1 to 3): 75,062 gal of 32-lb borate fluid (63,500 lb proppant).
2) Main (Phase 4): 36,023 gal of 32-lb borate fluid (59,600 lb proppant).
3) Fluid rheological properties at 100° F: n'=0.561 and K'=0.047 lb-s$^{n'}$/ft^2.

Table 2. Fluid and proppant volumes

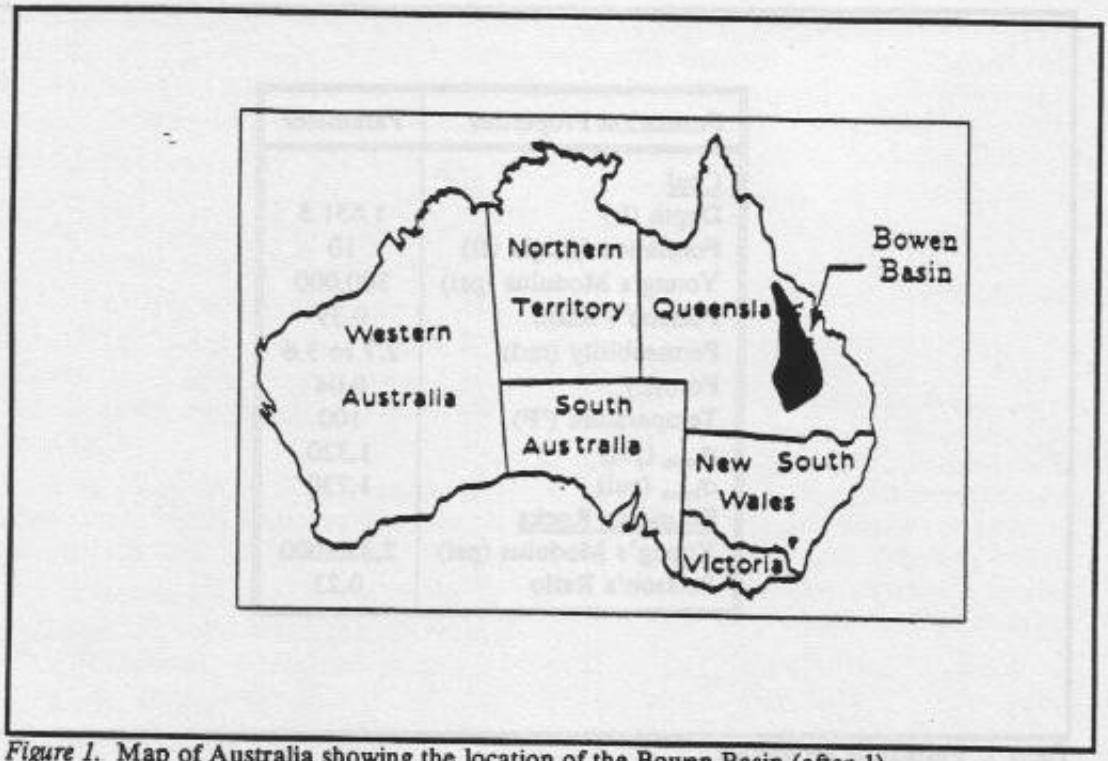

Figure 1. Map of Australia showing the location of the Bowen Basin (after 1)

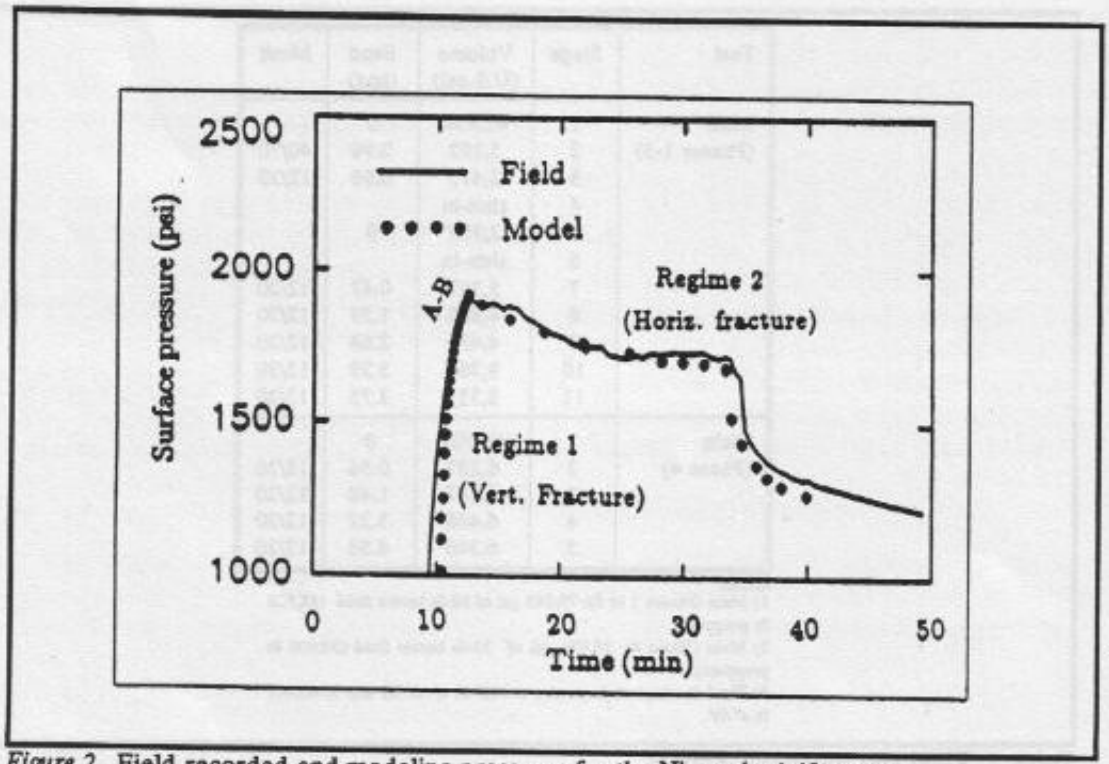

Figure 2. Field-recorded and modeling pressures for the Nipan 4 minifrac test

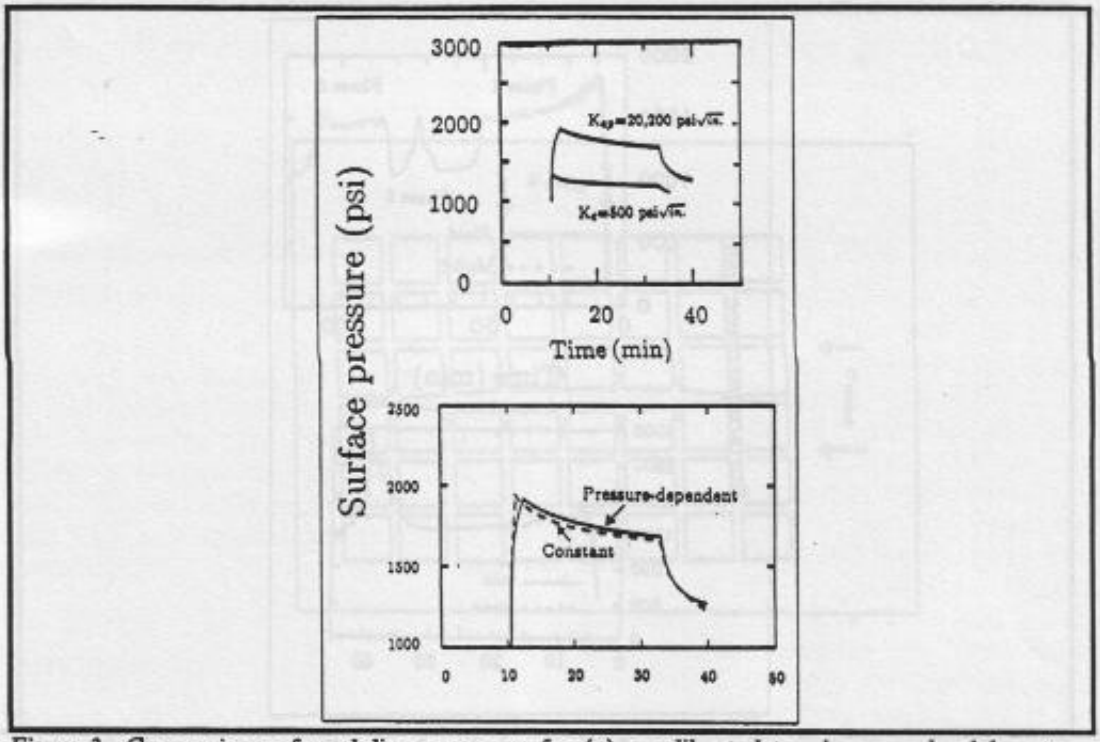

Figure 3. Comparison of modeling pressures for (a) a calibrated toughness and a laboratory-measured toughness; and (b) a constant fluid-loss coefficient and a pressure-dependent permeability function

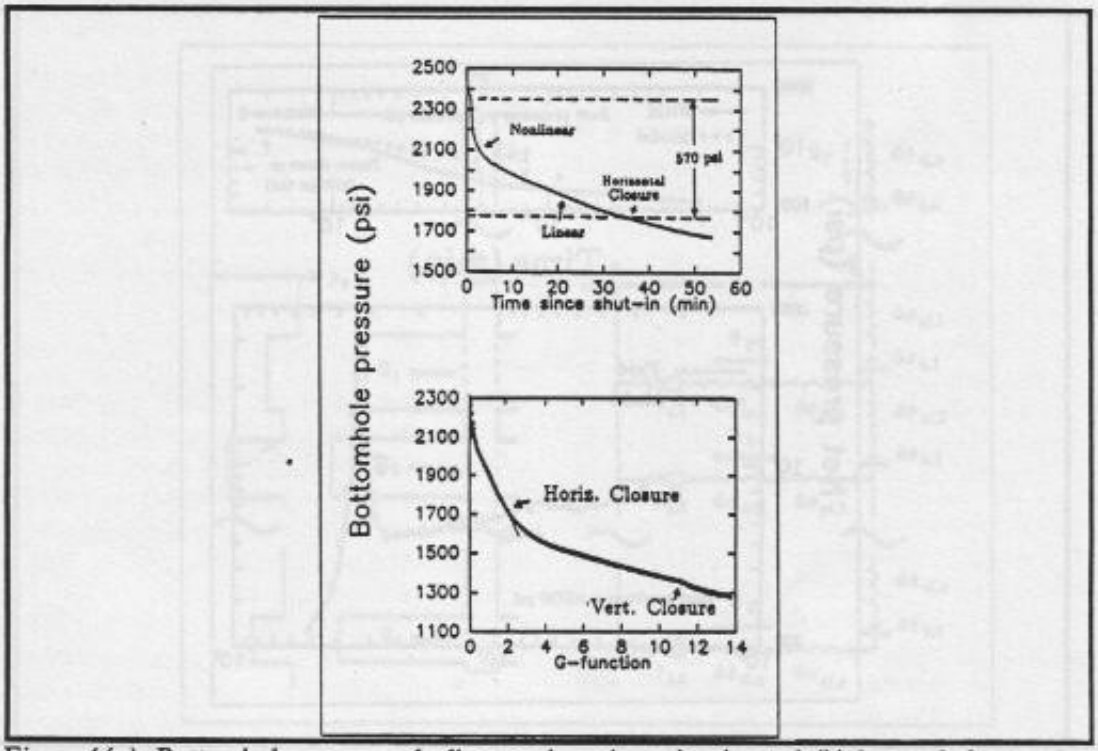

Figure 4.(a) Bottomhole pressure decline vs. time since shut-in, and (b) bottomhole pressure vs. G function for the minifrac test.

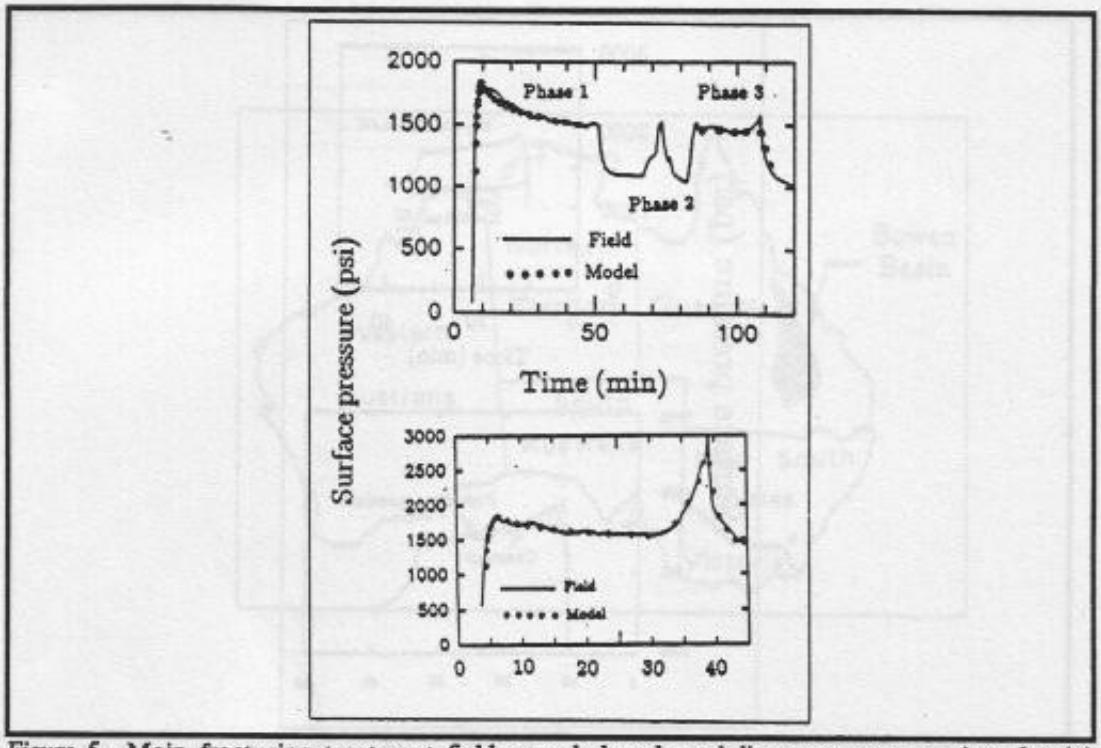

Figure 5. Main fracturing treatment field-recorded and modeling pressures vs. time for (a) Phases 1 through 3, and (b) Phase 4.

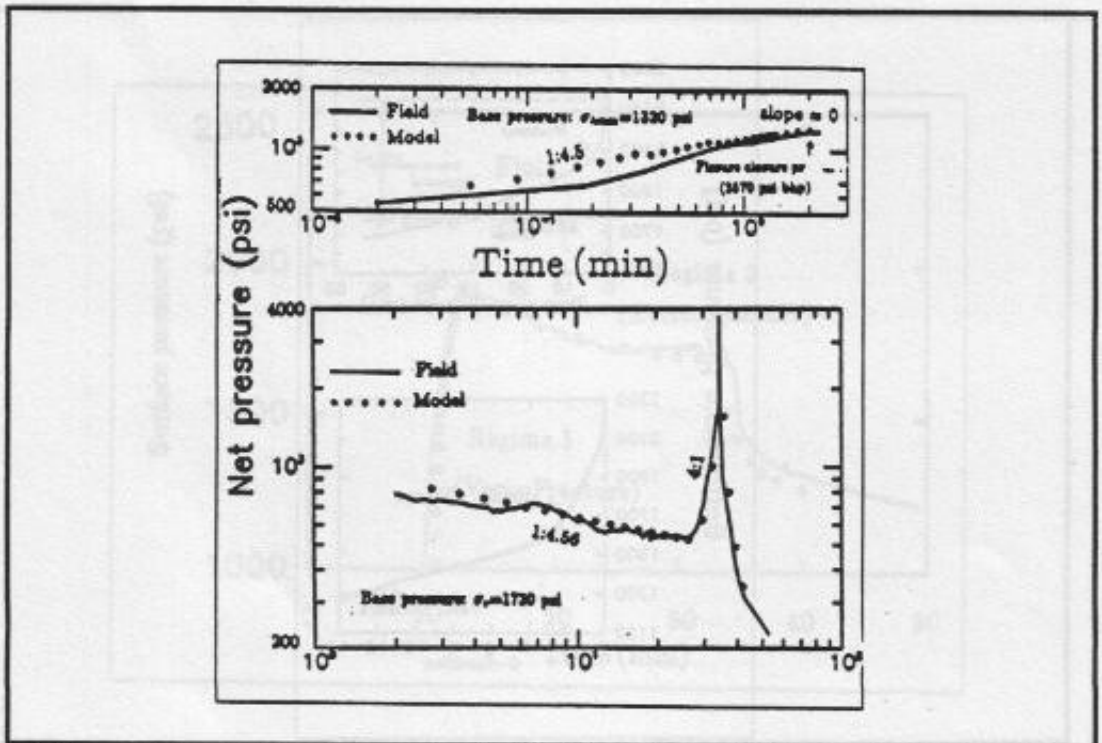

Figure 6. Net pressure vs. pumping time for the (a) vertical and (b) horizontal fractures propagated in Phase 4 of the main fracturing treatment

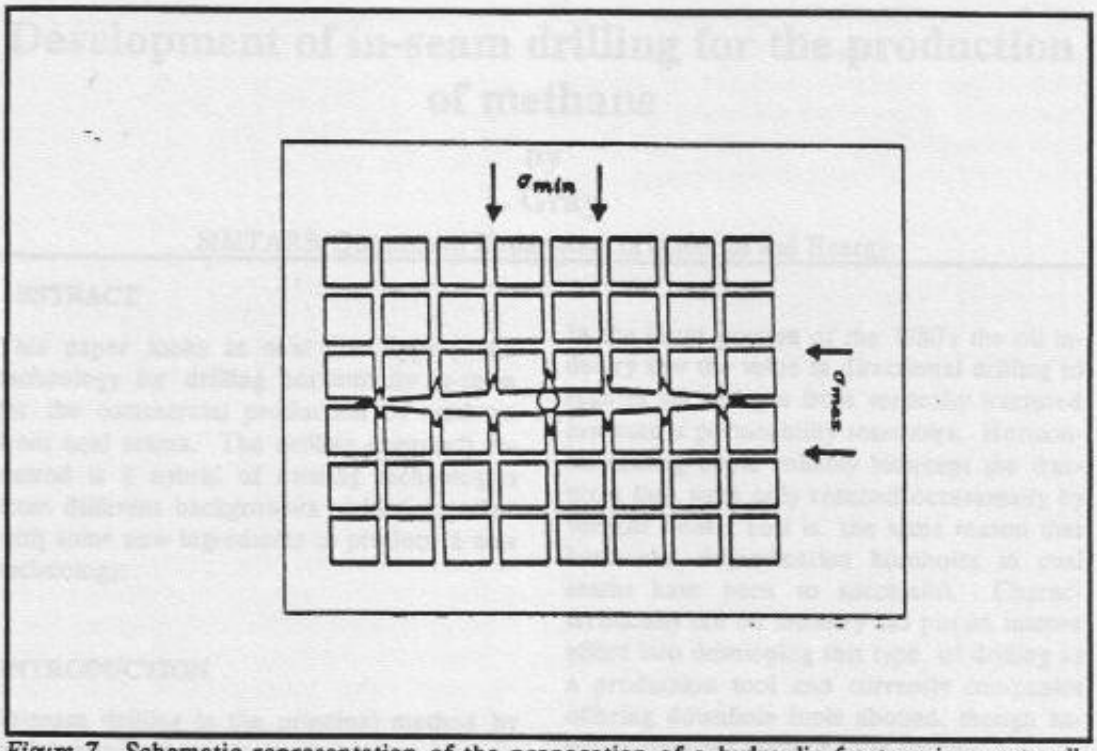

Figure 7. Schematic representation of the propagation of a hydraulic fracture in a naturally fractured reservoir

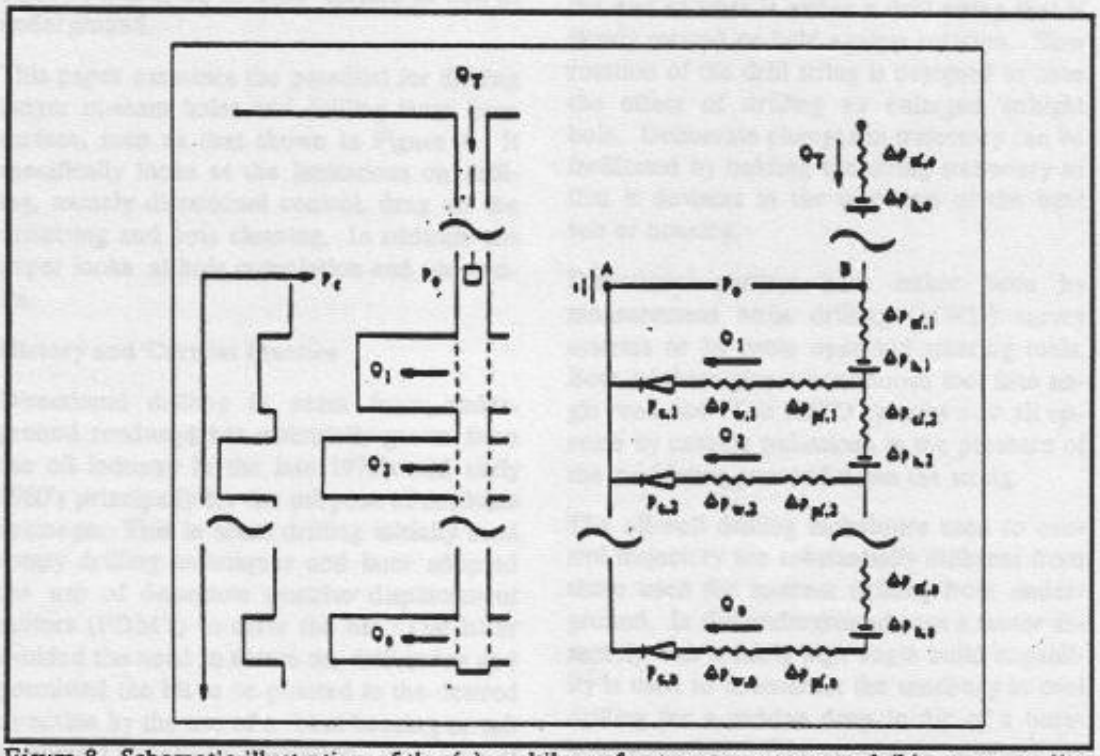

Figure 8. Schematic illustration of the (a) multilayer fracture treatment, and (b) corresponding electric circuit analogy (from 18).